Planar Hall Effect Sensors with Subnanotesla Resolution

A. Grosz[a)], V. Mor[a)], E. Paperno, S. Amrusi, I. Faivinov, M. Schultz, and L. Klein

***Abstract*—We report the fabrication of elliptical planar Hall effect sensors made of Permalloy with response determined by shape-induced uniaxial anisotropy. By using ac excitation and by optimizing the sensor thickness and the amplitude of the excitation current, we have obtained a magnetic field resolution which is better than 600 pT/√Hz at 1 Hz and close to 1 nT /√Hz at 0.1 Hz. We discuss possible routes for further improvement of the obtained resolution.**

***Index Terms*—Planar Hall effect, resolution, sensor, subnanotesla.**

I. Introduction

AMONG the wide range of magnetic sensors, those based on magnetoresistance (MR) effects are particularly attractive as they combine low cost, small size, and relatively high resolution at room temperature. Up to date, within the group of MR sensors, anisotropic magnetoresistance (AMR) sensors [1] hold the best resolution of 200 pT/√Hz at 1 Hz. Other promising results were obtained for example by using an ensemble of tunneling magnetoresistance (TMR) sensors [2] or by the integration of MEMS flux concentrators [3].

Planar Hall effect (PHE) sensors [4]-[6] have important intrinsic advantages compared to AMR sensors. PHE are sensors less sensitive to temperature drift [4], which limits the resolution at low frequencies. They are also much simpler compared to TMR or giant magnetoresistance (GMR) sensors, which comprise a stack of layers fabricated in complex processes. Such a layer stack also results in additional sources of noise, which is difficult to control and suppress [7].

Despite the advantages, so far the reported resolution of PHE sensors is lower than that of AMR sensors [1], [8]: 2 nT/√Hz at 1 Hz for the best PHE sensor in bridge configuration (PHEB) [6] and even worse in regular PHE sensors [10]. However, as we show in the present paper, PHE sensors can approach the resolution of AMR sensors at 1 Hz and surpass it at frequencies below 0.2 Hz. Furthermore, we point out routes that may further improve the resolution.

We also show in the present paper that, compared to miniature CMOS microfluxgates of comparable size and Hall effect sensors [9], the resolution of PHE sensors can be higher by one and three orders of magnitude, respectively.

To develop PHE sensors with improved resolution, we take the following approach: (i) we use an ac excitation current to translate the sensor output signal to frequencies where the 1/*f* noise of the electronic preamplifier can be neglected, (ii) guided by an analytical model, we optimize the thickness of the magnetic layer, and (iii) we optimize the amplitude of the excitation current.

II. Sensor Technology

A PHE sensor is usually fabricated so that in zero applied field the magnetization is parallel to the excitation current, flowing along the long sensor axis. This can be achieved via growth-induced magnetic anisotropy, either by growing the film in an applied magnetic field [4] or by exchange biasing the film with an antiferromagnetic layer [11]. These methods yield a single easy axis of magnetization and, consequently, uniform magnetization and its coherent rotation, when an in-plane magnetic field is applied perpendicular to the sensor easy axis.

Here, we use shape-induced anisotropy of elongated ellipses (see Fig. 1) to obtain anisotropy fields smaller than 10 Oe. The small anisotropy field increases the sensitivity of the sensor which reduces its equivalent magnetic noise.

We sputter Permalloy films capped with tantalum on Si substrates in a UHV-evaporation and sputtering system (BESTEC). We pattern the elliptical sensors using photolithography in a liftoff process. Gold leads and contact pads are deposited in the second stage.

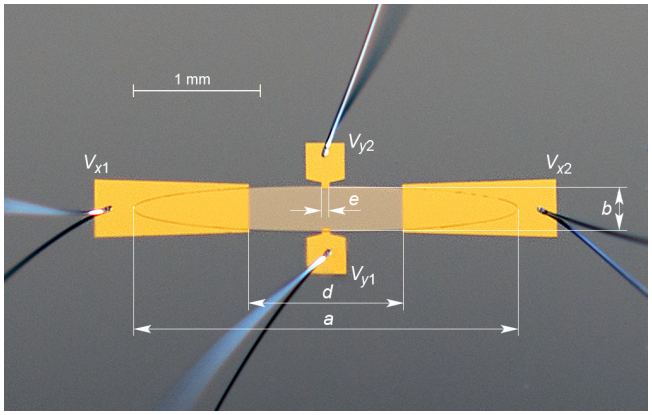

Fig. 1. A photograph of the PHE sensor. The elliptical part is made of Permalloy capped with tantalum. Excitation current is applied via the V_x gold terminals, and the output voltage is measured at the V_y terminals.

[a)]A. Grosz and V. Mor contributed equally to this work.

Manuscript received June 20, 2013. This work was supported in part by Analog Devices, Inc.

A. Grosz, E. Paperno, S. Amrusi, and I. Faivinov are with the Department of Electrical and Computer Engineering, Ben-Gurion University of the Negev, P.O. Box 653, Beer-Sheva 84105, Israel (corresponding author to provide phone: +972-52-897-0426; fax: +972-8-642-8677; e-mail: asaf.grosz@gmail.com).

V. Mor, M. Schultz, and L. Klein are with the Department of Physics, Institute of Nanotechnology and Advanced Materials, Bar-Ilan University, Ramat-Gan 52900, Israel.

It was shown [5] that elongated ellipses with aspect ratio $a/b>6$ behave as single magnetic domain particles with effective anisotropy field along the long axis even in relatively large ellipses with long axes in the millimeter range. Although it becomes more challenging as the probability of detrimental film imperfections in the ellipse increases with size.

The single magnetic domain behavior keeps the sensor gain stable and reproducible over time and also considerably reduces its 1/*f* noise [12].

III. Sensor Model

In polycrystalline ferromagnetic films, where crystal symmetry effects are averaged out, the longitudinal and transverse resistivities depend on the angle θ between the excitation current and the sensor magnetization as follows:

$$\rho_{xx} = \rho_{\perp} + \Delta\rho \cos^2\theta\,, \tag{1}$$

$$\rho_{xy} = \frac{1}{2}\Delta\rho \sin 2\theta\,, \tag{2}$$

where $\Delta\rho = \rho_{\parallel} - \rho_{\perp}$, $\rho_{\parallel}$ and $\rho_{\perp}$ are the resistivities parallel and perpendicular to the magnetization, respectively.

Equation (1) describes the AMR effect, whereas (2) describes the PHE.

The PHE resistivity is sensitive only to $\Delta\rho$, whereas the AMR resistivity is sensitive also to the resistivity and its temperature dependence [4].

The sensitivity of a PHE sensor when the applied magnetic field is smaller than the magnetic anisotropy can be expressed as follows [13]:

$$S_y = \frac{V_y}{B} = 10^4 \frac{V_x}{R_x}\cdot\frac{\Delta\rho}{t}\cdot\frac{1}{H_k + H_a}\,, \tag{3}$$

where V_y is the sensor output voltage, measured across the *y*-terminals, B is the applied magnetic field, V_x is the bias voltage across the *x*-terminals, R_x is the sensor resistance across the *x*-terminals, ρ is the sensor average electrical resistivity, t is the sensor thickness, H_k is the sensor shape induced anisotropy field, and H_a is the intrinsic anisotropy field.

The total noise of a PHE sensor has three main components (see Fig. 2): 1/*f* noise, thermal noise, and preamplifier noise:

$$e_{\Sigma} = \sqrt{V_x^2 \frac{\delta_H}{N_C \cdot Vol \cdot f^{\alpha}} + 4k_B T R_y + e_{amp}^2}\,, \tag{4}$$

where δ_H is the Hooge constant [12], N_C is the "free" electron density, equal to 1.7×10^{29} for $Ni_{80}Fe_{20}$ Permalloy [12], *Vol* is the effective volume, where the electrons are contributing to the conduction process in a homogeneous sample [12], f is the frequency, α is a constant, k_B is the Boltzmann constant, T is the temperature, R_y is the sensor resistance across the *y*-terminals, and e_{amp} is the total preamplifier noise, referred to its input (including the voltage noise, current noise, and the noise of the resistors).

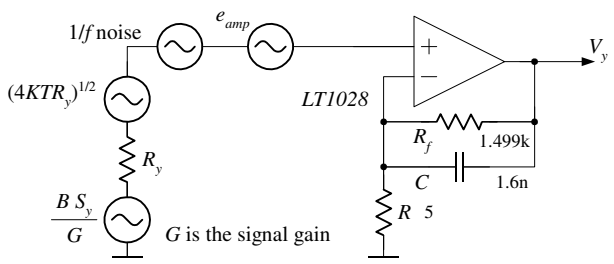

Fig. 2. The equivalent electrical circuit of the PHE sensor.

The sensor equivalent magnetic noise is defined as

$$B_{eq} = \frac{e_{\Sigma}}{S_y}\,. \tag{5}$$

For sufficiently low f and high V_x, the 1/*f* noise in (4) dominates, and the other noise components can be neglected. Consequently,

$$B_{eq} = \sqrt{\frac{\delta_H}{N_C \cdot Vol \cdot f^{\alpha}}}\,\frac{(H_k + H_a)\cdot t \cdot R_x}{10^4 \cdot \Delta\rho}\,. \tag{6}$$

For our elliptical sensors, in the limit [5], $a > b >> t$,

$$H_k \approx 10{,}807\frac{t}{b} \approx 10^4 \frac{t}{b}\,. \tag{7}$$

We turn now to the approximation of R_x, *Vol*, and R_y, assuming $t << a$, b, d, and e (see Fig. 1) that is valid for our sensors.

Neglecting the resistance of the gold leads and the interface resistance between the leads and the sensor, we approximate R_x by

$$R_x = \frac{C_1 \cdot \rho \cdot d}{t \cdot b}\,, \tag{8}$$

where we expect C_1 to be a constant not much larger than 1. Assuming that the relevant volume for *Vol* is an effective volume that contributes to the measured transverse voltage V_y, we approximate

$$Vol = C_2 \cdot t \cdot b \cdot e\,, \tag{9}$$

$$R_y = \frac{C_3 \cdot \rho \cdot b}{t \cdot e \cdot C_2}\,, \tag{10}$$

where C_3 similarly to C_1 is a constant not much larger than 1.

These constants are due to the interface resistance between the gold and Permalloy films, which increases the total value of R_y. C_2 is a constant larger than 1 that relates the real, rectangle shaped volume between the *y*-terminals to the effective conduction area.

We note that in our analysis we consider H_a, $\Delta\rho/\rho$, and ρ to be constants, which is justified for the range of thicknesses relevant for our sensors.

Equation (6) represents the minimum equivalent magnetic noise, because increasing V_x increases the sensor sensitivity in (3) and also, as mentioned above, the 1/*f* noise in (4) relative to the sensor thermal noise and the noise of the preamplifier, thus making them negligible.

By substituting (7)-(9) into (6) we obtain

$$B_{eq} = \sqrt{\frac{\delta_H}{N_C \cdot C_2 \cdot t \cdot b \cdot e \cdot f^{\alpha}}} \frac{\left(10^4 t + b \cdot H_a\right) \cdot C_1 \cdot d \cdot \rho}{10^4 \cdot \Delta\rho \cdot b^2}. \quad (11)$$

It is important to note that the equivalent magnetic noise in (11) depends only on the sensor dimensions and the material properties.

The optimal sensor thickness that minimizes (11) is:

$$t_{opt} = \frac{H_a \cdot b}{10^4}. \quad (12)$$

Interestingly, for this thickness:

$$H_k \approx H_a. \quad (13)$$

By substituting (12) into (11) we obtain the sensor low-frequency equivalent magnetic noise at the optimal thickness:

$$B_{\min} = \sqrt{\frac{\delta_H}{N_C \cdot C_2 \cdot e \cdot f^{\alpha}}} \frac{2\sqrt{H_a} \cdot C_1 \cdot d \cdot \rho}{10^2 \cdot \Delta\rho \cdot b^2}. \quad (14)$$

IV. Experiment

Guided by the above considerations, we have fabricated PHE sensors with aspect ratio *a*/*b*=8 (see Fig. 1). In principle, larger sensors are favorable for better resolution. The chosen dimensions are determined according to the capability to fabricate large ellipses without any detrimental imperfections. Accordingly, we have fabricated sensors with *a*=3 mm. The distance *d* between the current leads should be as small as possible to decrease the resistance R_x. On the other hand, if the leads are too close a significant part of the current would flow through V_y leads instead of flowing through the magnetic layer which would decrease significantly the PHE signal. Therefore we chose *d*=1.2 mm and *d*/*e*=20.

The sensor parameters are listed in Table. I. The values of $\Delta\rho/\rho$, ρ, and H_a were determined by measurements as described in [5].

TABLE I
Parameters of the optimized PHE sensor experimental model

Parameter	Value	Units	Parameter	Value	Units
a	3	mm	H_a	3.84	Oe
b	0.375	mm	H_k	3.45	Oe
t	120	nm	$\Delta\rho/\rho$	1.6	%
d	1.2	mm	ρ	$2.7\ 10^{-7}$	Ohm·m
e	0.06	mm	α	1.5	
R_x	9.97	Ohm	δ_H	$2.73\ 10^{-3}$	
R_y	5.08	Ohm	N_c	$17\ 10^{28}$	$1/m^3$
I_x	71.4	mA			

The sensor was excited with ac current. The sensor output was amplified using a low-noise operational amplifier (LT1028). The amplifier output was sampled by a 24-bit ADC (PXI-5421) and demodulated using a digital synchronous detector. An 100 Hz low-pass filter at the output of the synchronous detector was used to band-limit the signal.

As the input voltage noise of the LT1028 operational amplifier flattens at around 1 kHz, we have excited the sensor at 1.22 kHz to avoid the amplifier 1/*f* noise and 50 Hz power network harmonics.

The sensor gain S_y was measured using a calibrated solenoid and was found to be flat from 10 mHz to 100 Hz.

The sensor noise was measured by using a seven layer magnetic shield to suppress low-frequency interferences. To find the optimal excitation current, we have changed it by small steps measuring at each step the sensor gain and noise.

Theoretically, if the sensor power consumption is not limited, the excitation current should be as high as possible to bring the equivalent magnetic noise to a minimum at all frequencies. However, the ability of the sensor to dissipate the excessive heat is limited and, therefore, at a too high current, the sensor becomes thermally unstable, which degrades its equivalent magnetic noise.

From measurements of R_x, we have found C_1=1.38 according to Eq. (8), where *r*, *d*, *t*, and *b* are known. To find C_2=4.23, we have simulated with COMSOL software R_y according to (10), where C_3=1, because the simulation does not consider the interface resistance between the gold and Permalloy films. Then by substituting C_2 into (10) and comparing it to the measured value of R_y, we have determined C_3=1.53.

Fig. 3 shows the sensor equivalent magnetic noise for the case of too low (35.7 mA), optimal (71.4 mA), and too high (83.3 mA) excitation currents, I_x.

The measured equivalent magnetic noise in nT/√Hz is fitted as follows:

$$B_{eq} = a_0 + a_1 \cdot \frac{1}{f^{0.75}}, \quad (16)$$

with a_0=0.83 and a_1=0.14 for I_x=35.7 mA; a_0=0.4 and a_1=0.17 for I_x=71.4 mA; a_0=0.35 and a_1=0.24 for I_x=83.3 mA.

One can see from Fig. 3 that the sensor equivalent magnetic

noise at the optimal excitation current is either the lowest one or does not practically differ from the noise values at the other excitation currents. A too low excitation current provides similar results at low frequencies but worse results at higher frequencies, where the 1/f noise is not so dominant. At a too high excitation current, the equivalent magnetic noise at high frequencies is similar to that of the optimal current, but is degraded at low frequencies due to thermal drift.

From the obtained results for the optimal current we estimate the Hooge constant $\delta_H=2.73\times10^{-3}$. This value differs only by 36% from the so called "Hooge magic number" of 2×10^{-3} which was vastly reported as the Hooge constant for single layer metal films in general [14], and magnetic films in particular [12].

We have built and tested three additional identical sensors and have found that their noise and sensitivity do not differ by more than 10% from the sensor described above.

The white noise components, e.g. thermal and preamplifier noise, degrades the sensor optimal equivalent magnetic noise by 40% at 0.1 Hz, 300% at 1 Hz and more than 1000% at 10 Hz. Although our preamplifier has a very low noise of 1 nV/√Hz, it is still three times larger than the thermal noise of the sensor (0.29 nV/√Hz). Therefore, we expect a significant improvement in the equivalent magnetic noise by using a lower noise preamplifier [16], especially at higher frequencies. Further improvement in the equivalent magnetic noise is possible due to the following. The highest $\Delta\rho/\rho$ value for our sensors is about 1.6%, which may be increased up to 4% by using an insulation layer, consisting of a thermal silicon dioxide or a low stress silicon nitride deposited by a PECVD process at low temperatures [16]. Ferromagnetic nitride films exhibiting $\Delta\rho/\rho$ on the order of 6% [17] can also be considered. Increasing $\Delta\rho/\rho$ by a factor of 2 and decreasing H_a by a factor of 5 [17] is expected to improve the equivalent magnetic noise by a factor of 4.5.

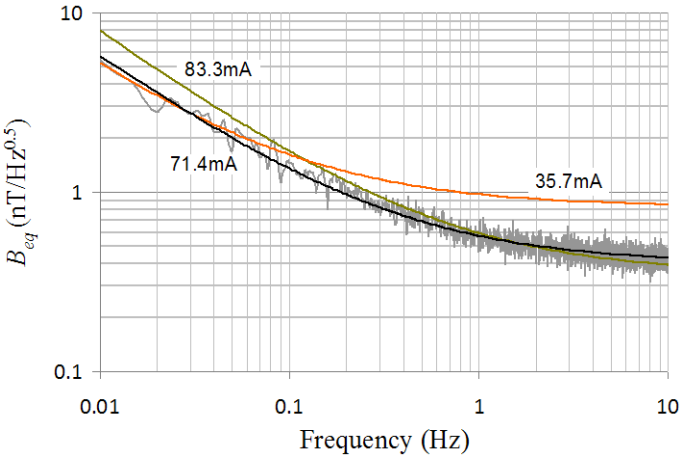

Fig. 3. Equivalent magnetic noise versus frequency. For the optimum excitation current amplitude of 71.4 mA, both the sensor noise and the noise fit are shown. For other excitation current amplitudes only the noise fits are shown.

V. Conclusion

By exciting the sensor with an optimized ac current and optimizing the sensor thickness, we have decreased the sensor 1/*f* noise drastically and improved its resolution at low frequencies. The obtained resolution 570 pT/√Hz at 1 Hz, is by 3.5 times better than the best results [6] reported for the PHE sensors. From 0.2 Hz and below, it is also better than the resolution of the best AMR sensors [1], [8].

References

[1] N. A. Stutzke, S. E. Russek, and D. P. Pappas, "Low-frequency noise measurements on commercial magnetoresistive magnetic field sensors," *J. Appl. Phys*., vol. 97, pp. 10Q107-1–10Q110-3, 2005.

[2] S. H. Liou et al., "Picotesla Magnetic Sensors for Low-Frequency Applications," *IEEE Trans. Magn*., vol. 47, pp. 3740-3742, 2011.

[3] J. Hu, W. Tian, J. Z., M. Pan, D. Chen, and G. Tian, "Remedying magnetic hysteresis and 1/f noise for magnetoresistive sensors," *Appl. Phys. Lett*., vol. 102, pp. 054104-1–054104-4, 2013.

[4] A. Schuhl et al., "Low-field magnetic sensors based on the planar Hall effect," *Appl. Phys. Lett*., vol. 66, pp. 2751-2753, 1995.

[5] V. Mor, et al., "Planar Hall effect sensors with shape-induced effective single domain behavior," *J. Appl. Phys*., vol. 111, pp. 07E519-1–07E519-3, 2012.

[6] A. Persson, et al. "Modelling and design of planar Hall effect bridge sensors for low-frequency Applications," *Sensors and Actuators A*, vol. 189, pp. 459-465, 2013.

[7] Z. Q. Lei et al., "Review of noise sources in magnetic tunnel junction sensors," *IEEE Trans. Magn*., vol. 47, pp. 602-612, 2011.

[8] HMC1001/HMC1002 Magnetic Sensors, Honeywell.

[9] P. Ripka and M. Janosek, "Advances in magnetic field censors," IEEE Sensors Journal, vol. 10, pp. 1108-1116, 2010

[10] F. Montaigne, A. Schuhl, F. Nguyen Van Dau, and A. Encinas, "Development of magnetoresistive sensors based on planar Hall effect for applications to microcompass," *Sensors and Actuators A*, vol 81, pp. 324-327, 2000.

[11] A. Nemoto, Y. Otani, S. G. Kim, and K. Fukamichi, "Planar Hall resistance ring sensor based on NiFe/Cu/IrMn trilayer structure," *Appl. Phys. Lett. A*, vol. 74, pp. 4026-4028, 1999.

[12] M. A. M. Gijs, J. B. Giesbers, J. W. van Est, J. Briaire, L. K. J. Vandamme, and P. Beliën, "1/*f* noise in magnetic Ni80Fe20 single layers and Ni80Fe20/Cu multilayers," *Journal of Magnetism and Magnetic Materials*, vol. 165, pp. 360-362, 1997.

[13] L.W. Ejsing, *Magnetic Beads in Microfluidic Systems*, Ph.D. thesis, Technical University of Denmark, 2006.

[14] M. Ziese, M. J. Thornton, *Lecture Notes in Physics*, Springer-Verlag, Berlin, Heidelberg, p. 569, 2001.

[15] Felix A. Levinzon, "Ultra-low-noise high-input impedance amplifier for low-frequency measurement applications," *IEEE Trans. on Circuits and Systems-I*, vol. 55, pp. 1815- 1822, 2008.

[16] H. Hauser, G. Stangl b, J. Hochreiter, "High-performance magnetoresistive sensors," *Sensors and Actuators A*, vol. 81, pp. 27-31, 2000.

[17] R. Loloee, "Epitaxial Ni_3FeN thin films: A candidate for spintronic devices and magnetic sensors," *J. Appl. Phys*. vol. 112, pp. 023902-1–023902-6, 2012.